Journal of Sound and Vibration (1998) **212**(4), 649–662

ANALYSIS OF LOSSES DUE TO ROTOR VIBRATIONS IN A HIGH-T_c SUPERCONDUCTING FLYWHEEL SYSTEM

A. TONOLI

Dipartimento di Energetica, *Politecnico di Torino*, *Corso Duca degli Abruzzi* 24, 10129 *Torino*, *Italy*

AND

H. J. BORNEMANN

Forschungszentrum Karlsruhe GmbH, *INFP*, *P.O. Box* 3640, 76021 *Karlsruhe*, *Germany*

(*Received* 7 *May* 1997, *and in final form* 2 *December* 1997)

The loss mechanisms associated with the combined effects of magnetic unbalance and hysteretic damping in a superconducting flywheel system have been modelled under the assumption that the dynamic characteristics of the bearing can be approximated by a linear, elastic isotropic spring with structural damping. The theoretical rundown equation of motion of such systems has been obtained by a Lagrangian approach, neglecting the effects of angular acceleration. The unknown parameters of the theoretical model have been determined by two different identification procedures starting from experimental time versus rotational speed curves obtained during rundown tests performed on a plastic flywheel with embedded permanent magnet, suspended on a high T_c superconducting stator. In addition to magnetic friction and eddy current losses, the hysteretic nature of the superconducting magnetic bearing gives a significant contribution to the overall losses. Accordingly, the efficiency of the system can be increased by minimizing the unbalance of the rotor.

1. INTRODUCTION

The application of magnetic bearings based on high critical temperature (T_c) superconductors seems very promising for the levitation of flywheels designed for a variety of applications requiring long-term storage of mechanical energy. The autostable behaviour of these bearings is one of their main advantages over active magnetic bearings, especially in applications which are exceptionally critical concerning friction losses and safety of operation. Low friction losses and safety of operation are crucial aspects in view of the high amount of kinetic energy that can be stored in the flywheel.

At present, practical bearing designs have been made possible by the development of the melt texturation process leading to a considerable improvement in the interaction forces that can be developed between $YBa_2Cu_3O_7$ (YBCO) based high T_c superconductor (HTS) bulk components and permanent magnets. The need of cryogenic temperatures for their operation does not seem to constitute a major drawback due to both the low cost of liquid nitrogen and to the standard technology involved in its management.

Studying the mechanical interaction between a type II superconductor and a permanent magnet, Brandt [1] gives evidence that if the amplitude of the motion remains smaller than

0022–460X/98/190649 + 14 $25.00/0/sv971457

a given threshold, the system performs in a basically conservative manner. Whenever the amplitude of the motion overcomes the threshold, the restoring forces become hysteretic and an amount of energy is dissipated at each cycle. The transition between conservative and dissipative behaviour seems to be a function of the critical current and the flux pinning capability of the superconductor, and of the gradient of the magnetic field. From a macroscopic point of view, the transition from conservative to dissipative behaviour is analogous to the transition between "elastic" to "plastic" behaviour and can be modelled as suggested by Hull *et al*. [2] in terms of a linear spring connected in series with an ideal dry friction element.

For applications such as long-term kinetic energy storage within a flywheel, a detailed analysis of the energy dissipating mechanisms occurring in the bearings is very important for the optimization of the system. Although the dissipative behaviour of the bearing forces is very useful to limit the high whirling amplitudes when corssing the critical speeds and to increase the instability thresholds [3], it is a drawback during non-critical operating conditions because of non-negligible kinetic energy dissipation.

The influence of dissipations within the bearings due to the whirling of the rotor on its rotating speed has been measured by Genta *et al*. [4], during a rundown test performed on a small rotor supported by superconducting magnetic bearings. The sharp deceleration observed when crossing the critical speed has been ascribed to the effects of unbalance and to the damping properties of the bearings.

Investigating other sources of dissipations such as aerodynamic drag and eddy current losses in small rotating permanent magnets suspended in vacuum conditions above a cylindrical HTS stator, Weinberger *et al*. [5] demonstrate the existence of a frequency independent drag torque that is assigned to "slight magnetic asymmetries" in the permanent magnet.

The aim of the present paper is to investigate the energy dissipation occurring in a superconducting flywheel due to the combined effects of unbalance and hysteretic damping. The whirling motion of the flywheel is modelled using a simple Jeffcott rotor. A complex stiffness approach is adopted to take into account the hysteretic characteristics of the bearings. The rundown equation of motion of the system is then obtained by a Lagrangian approach assuming negligible effects of the angular acceleration. Due to the lack of a direct measurement at the operating conditions of rotating speed and whirling amplitude [6, 7], the unknown parameters of the theoretical model are identified from the experimental data measured during rundown tests performed on the flywheel. The identified parameters are the critical speed, the bearing loss factor and the unbalance. To reduce the losses due to eddy currents and to aerodynamic drag, the tests were performed in high vacuum with a plastic flywheel disc.

2. EXPERIMENTAL SET-UP

The flywheel system employed during the experimental tests is shown in Figure 1. It was built at Forschungszentrum Karlsruhe and is made of an unpierced Plexiglass disc (FD) with an outer diameter of 190 mm, and a Nd–Fe–B ring shaped permanent magnet fitted in a groove so that the resulting assembly has a constant thickness of 30 mm. The outer and inner diameters of the permanent magnet are 90 mm and 60 mm respectively, and its thickness is 15 mm [8].

Taking into account that the aim of the set-up is to investigate the loss mechanisms within the flywheel system rather than that of optimizing the centrifugal stress distribution

and the kinetic energy density, the constant overall thickness configuration had been chosen to simplify the analysis and construction as much as possible.

Six melt-textured $YBa_2Cu_3O_7$ pellets (SC) with a diameter of 34 mm and a thickness of 18 mm, mounted in a closed cryostat cooled by a continuous flow of liquid nitrogen, constitute the stator of the superconducting magnetic bearing. A non-conductive fibreglass cryostat was employed to differentiate the losses due to the eddy currents induced by the asymmetries in the field of the ring magnet from any other losses inherent to the bearing system. A special gluing and sealing technique suitable to withstand the high vacuum and low temperature during operation was developed for this application. To reduce the gap between rotor and stator of the bearing, the lid of the cryostat is only 0·4 mm thick. Thin-walled, stainless steel bellows are used as LN_2 feed lines.

The driving unit consists of a drive shaft connecting the flywheel to a high speed asynchronous motor/generator (M/G) via a mechanical clutch. A flexible coupling was placed at the drive shaft–motor interface to compensate for any runout between the axes of rotation of the flywheel and of the motor and to reduce the first critical speed of the flywheel during operation of the motor.

At the beginning of the test, the flywheel is connected to the drive shaft; after it has been spun up to the desired speed, the motor is moved up by a spring-loaded mechanism. The mechanical clutch at the lower end of the drive shaft is thus disengaged and the flywheel disc is freely rotating. Even though this configuration makes it impossible to re-connect the flywheel before it has come to a complete stop, it has been chosen because it allows one to test rotors of different materials and shapes, avoiding any interaction with the driving unit during the rundown.

To allow an easy see-through operation, the vacuum-proof flywheel housing was made of Plexiglass. The pressure within the vacuum chamber and the temperature of the stator of the motor are monitored continuously during the tests. The rotating speed of the flywheel is measured by a non-contacting optical sensor and stored in a PC.

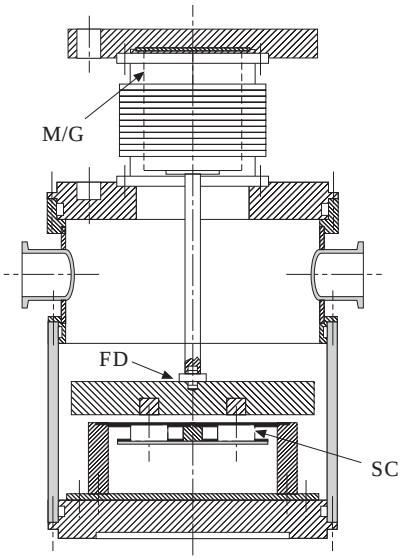

Figure 1. A schematic of the superconducting flywheel system. M/G, motor/generator; FD, flywheel disk; SC, superconducting pellets.

3. ANALYSIS OF THE BEARING LOSSES

3.1. EDDY CURRENT LOSSES

Eddy current losses are induced in any conducting material that is subject to a time varying magnetic field. No eddy currents can then be induced within the Plexiglass part of the flywheel and the fibreglass lid of the cryostat. Therefore the main part of these losses can take place only within the ring magnet.

The magnetic flux density trapped by one of the six pellets of the bearing stator has been measured after field cooling at a distance of 1·6 mm from the surface of a 30 mm × 30 mm × 6 mm Nd–Fe–B permanent magnet developing a maximum magnetic flux of 0·2 T at the centre of its main faces. The trapped flux measured at a distance of 0·5 mm from the surface of the sample in a direction parallel to its axis shows a maximum value of about 0·1 T at the centre of the pellet, while it is nearly null on its edges. Even in the ideal case when the same field is trapped by each pellet, the arrangement of six discrete pellets within the bearing stator will give way to a varying circumferential field distribution.

When the ring magnet is rotating at a speed ω over the bearing stator, it is subject to a magnetic field varying with an angular frequency 6ω. Due to the conducting nature of the magnet, eddy currents are induced.

The quantitative evaluation of the eddy current losses within the rotating magnet is far from being straightforward. Nevertheless, the dissipated power is proportional to the square of the rotating speed ω and to the gradient B_α of the magnetic flux density in circumferential direction:

$$P_{ec} \propto \frac{1}{\rho}\,\omega^2 B_\alpha \tag{1}$$

where ρ is the electric resistivity of the material of the ring magnet. The dissipated power P_{ec} corresponds to a drag torque Γ_{ec}:

$$P_{ec} = \omega\Gamma_{ec} \;\Rightarrow\; \Gamma_{ec} \propto \frac{1}{\rho}\,\omega B_\alpha. \tag{2}$$

The eddy currents in the ring magnet induce a drag torque proportional to the rotating speed, contributing to the so-called ''frequency dependent losses'' [9, 10]. The drag torque Γ_{ec} can be reduced by increasing the resistivity of the permanent magnet, or by reducing the inhomogeneities of the magnetic field in circumferential direction.

3.2. AERODYNAMIC LOSSES

In the 10^{-4} torr pressure range, the aerodynamic losses are determined by the interaction between the residual gas molecules and the flywheel surface. The drag torque resulting from this interaction was found to be proportional to the rotating speed ω [10, 11].

3.3. MAGNETIC FRICTION

As shown previously [2, 5, 12], a torque independent of rotating speed is needed to rotate a permanent magnet over a superconductor. This torque is due to the asymmetries in the field of the permanent magnet and can be viewed as a sort of dry friction.

3.4. DAMPING LOSSES CAUSED BY ROTOR UNBALANCE

It is well known that the typical force–displacement characteristics of a permanent magnet moving with respect to a superconducting pellet are irreversible. This results in a hysteresis cycle the shape of which depends strongly upon the amplitude of displacement

[2, 4, 7, 12, 14–17]. If the displacements between the superconducting pellet and the magnet are small relative to their size, the force–displacement characteristics are to a good approximation elliptical, and the bearing can then be modelled as a spring affected by structural damping.

At a microscopic level, hysteresis occurs whenever the displacement of a type II superconductor in an inhomogeneous magnetic field is large enough to induce "unpinning" of the flux lines [1]. Only in the limiting case, when displacements are small enough, does unpinning not occur and the interaction force become conservative.

In the case of harmonic displacements, the mechanical characteristic of a spring affected by structural damping can be represented in terms of a complex stiffness of amplitude K and loss factor η [3]. Due to the small angular accelerations measured during a rundown test, the flywheel is subject to a circular synchronous whirling that can be decomposed in harmonic displacements along the x and y directions lying on its mid-plane. The bearing force can then be approximated using the complex stiffness notation as

$$F_{brg} = K\,\mathrm{e}^{-\imath\eta} z, \tag{3}$$

where $\imath = \sqrt{-1}$ and the x and y displacements have been assembled in the complex displacement $z = x + \imath y$. The real and imaginary parts of F_{brg} represent the components of the bearing force along the x and y directions respectively.

Due to the unavoidable presence of an unbalance, the rotating flywheel is subject to a whirling motion. Assuming the amplitude of the whirling motion to be large enough to induce unpinning of flux lines, the bearing restoring forces are hysteretic and energy is dissipated during each cycle. The dissipation is referred to as "unbalance losses".

If the flywheel is subject to a whirling motion of amplitude Z_0 and phase φ,

$$z = Z_0\,\mathrm{e}^{\imath(\omega t + \varphi)}, \tag{4}$$

and assuming that the loss factor η is small enough so that $\sin\eta = \eta$, the energy dissipated by hysteresis at each cycle $2\pi/\omega$ is

$$W_{diss} = \oint \mathbf{F}\cdot \mathrm{d}\mathbf{z} = \int_0^{2\pi/\omega} K\,\mathrm{e}^{-\imath\eta}\dot{\bar{z}}z\,\mathrm{d}t \approx -2\pi K Z_0^2\eta \leqslant 0, \tag{5}$$

where $\bar{z}$ is the conjugate of z. W_{diss} is a function of the amplitude of the whirling motion and of the loss factor η but not of the rotating speed ω. If the losses within the bearing had been modelled by means of a linear viscous damping model, the energy dissipated in a cycle would have been also a function of the rotating speed.

Due to the high unbalances that usually affect rotors suspended by superconducting bearings, the energy dissipated during whirling motions must be taken into account to describe the flywheel behaviour during a rundown test or to determine the power needed to keep it at constant rotating speed.

A simple model commonly used to analyze the unbalance losses in a rotor–bearing system is the so called Jeffcott rotor (Figure 2). It consists of a rigid disc with mass m which has an eccentricity ϵ from point C, where both the elastic and the damping forces developed by the bearing act.

The Jeffcott model can be used to describe the rundown behaviour of the flywheel system under the following assumptions. (i) *The gyroscopic effects are negligible*: even if this assumption is not exactly valid in the present case, the flywheel is thin enough to reduce the errors to a minimum. (ii) *Angular accelerations are small*: since a typical rundown test, starting from 5500 rpm, lasts for several hours, the flywheel can be thought to reach steady state conditions at each rotating speed during the rundown. (iii) *The behaviour of the*

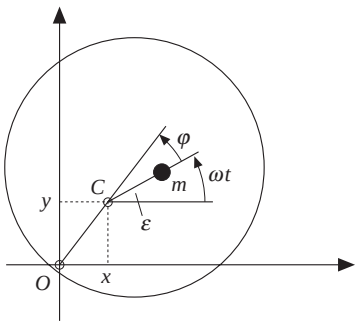

Figure 2. The Jeffcott rotor. $Oxyz$, inertial reference frame; C, point at which the elastic and the damping forces of the bearing act; m, mass of the disc located at the centre of gravity; ϵ, eccentricity.

bearing is linear: this is valid if the displacements remain small. (iv) *The restoring force is axis symmetric*: this holds both for what the elastic and the damping characteristics of the bearing is concerned and is justified by the symmetrical arrangement of the superconducting pellets, their rather homogeneous characteristics and by the symmetry of the ring magnet.

The flexural behaviour of such a system can be described by the following equation of motion:

$$m\ddot{z} + K\,\mathrm{e}^{-\imath\eta}z = m\epsilon\omega^2\,\mathrm{e}^{\imath\omega t}. \tag{6}$$

The steady state solution of the above equation is a circular synchronous whirling [3]:

$$z = \epsilon\,\frac{\omega^2}{\sqrt{(\omega_c^2 - \omega^2)^2 + \eta^2\omega_c^4}}\,\mathrm{e}^{\imath(\omega t + \varphi)}, \tag{7}$$

where $\omega_c = \sqrt{K/m}$.

In principle, equation (7) is a solution of the equation of motion (6) only in the case of a constant rotating speed ω. However, owing to the assumption of small angular accelerations, it is valid also in the case of a rundown test.

The coupling between lateral motion and rotating speed during a rundown test can be determined using a Lagrangian approach. With the flywheel being the only part included in the system, the magnetic bearing forces and the drag torques are accounted for as external forces acting on it. The circular whirling (7) has been considered as a constraint acting on the x and y displacements. The only remaining degree of freedom of the rotor is then the rotation $\vartheta = \omega t + \varphi$, which is considered as the Lagrangian co-ordinate of the system. With the assumption of small angular acceleration, the kinetic energy of the rotor can be expressed as

$$T = \tfrac{1}{2}(mZ_0^2 + I_p)\omega^2, \qquad \omega = \dot{\vartheta}. \tag{8}$$

In practical operating conditions the whirling amplitude is such that the contribution mZ_0^2 to the polar inertia of the rotor can be neglected compared to I_p. The kinetic energy can then be approximated as

$$T \approx \tfrac{1}{2}I_p\omega^2. \tag{9}$$

The Lagrangian generalized force Q_ϑ has been computed taking into account the contributions given by the bearing lateral force $\mathbf{F}_{brg}$, the aerodynamic drag, the eddy current and the magnetic friction:

$$Q_\vartheta = c_0 + c_1\omega + \mathbf{F}_{brg} \cdot \frac{\partial \mathbf{z}}{\partial \vartheta}. \tag{10}$$

The constant c_0 accounts for the frequency independent losses due to magnetic friction, while c_1 accounts for the combined effects of eddy current losses and molecular drag.

Substituting the bearing force (3) and the whirling motion (7) in (10), the Lagrangian component Q_ϑ can be written as

$$Q_\vartheta = c_0 + c_1\omega - \eta \frac{(m\epsilon\omega_c)^2}{m[(\omega_c^2 - \omega^2)^2 + \eta^2\omega_c^4]}\omega^4. \tag{11}$$

Due to the choice of considering the flywheel as the only part included in the expression of the Lagrangian function, the only potential energy of the system is stored in gravitational form. The elastic potential of the bearing is not included in the Lagrangian, as the bearing forces are considered as external forces and their contribution is taken into account through the generalized force Q_ϑ. During the experiments the vertical displacements of the flywheel are negligible: the gravitation energy is constant and therefore does not contribute to the system dynamics.

Lagrange's equation of motion becomes

$$\frac{\mathrm{d}}{\mathrm{d}t}\left(\frac{\partial T}{\partial \dot{\vartheta}}\right) - \frac{\partial T}{\partial \vartheta} = Q_\vartheta. \tag{12}$$

Substituting equations (9) and (11) in equation (12), the rundown equation of motion turns out to be

$$I_p\dot{\omega} = c_0 + c_1\omega - \eta \frac{(m\epsilon\omega_c)^2}{m[(\omega_c^2 - \omega^2)^2 + \eta^2\omega_c^4]}\omega^4. \tag{13}$$

The subcritical and the supercritical speed ranges are characterized by substantially different forms of behaviour. (i) In subcritical conditions ($\omega \ll \omega_c$) the Lagrangian force due to the rotor whirling motion is negligible compared to those due to the aerodynamic, the eddy current and the magnetic drag. In this case the angular acceleration is a linear function of the rotational speed ω:

$$\omega \ll \omega_c \;\Rightarrow\; I_p\dot{\omega} \approx c_0 + c_1\omega. \tag{14}$$

(ii) In supercritical conditions ($\omega \gg \omega_c$) the unbalance losses become independent of the rotational speed. They contribute to the frequency independent losses:

$$\omega \gg \omega_c \;\Rightarrow\; I_p\dot{\omega} \approx c_0 - \frac{\eta(m\epsilon\omega_c)^2}{m} + c_1\omega. \tag{15}$$

In high supercritical conditions, the amplitude of the whirling tends to be independent of the rotational speed ω. Then the power dissipated by the hysteretic nature of the bearing becomes proportional to the number of whirling cycles per unit time, and thus to the rotating speed. In other words, at constant ω a dissipated power proportional to the rotating speed is equivalent to a constant drag torque acting on the flywheel.

Unless the rotor unbalance $m\epsilon$ is negligible, the losses due to the rotor unbalance give a substantial contribution to the overall dissipation. In the supercritical speed range they can overcome those due to eddy currents, aerodynamic drag and magnetic friction. Due

to the low stiffness values usually obtained in a superconducting magnetic suspension, the rotor is operated in supercritical conditions most of the time. Accurate balancing is then necessary to reduce the losses within it.

While for conventional bearings the axis of the geometric centre is also the elastic axis of the rotor, in superconducting bearings the elastic axis C of the suspension is related to the magnetic symmetry axis of the bearing. In this case, the eccentricity ϵ is the distance between the rotor centre of gravity and the magnetic axis. The unbalance is closely related to the difficulty in producing permanent magnets and superconducting stators with highly symmetrical field distributions. For our experiments, balancing was achieved by shifting the centre of gravity into the elastic axis.

4. IDENTIFICATION OF THE SYSTEM PARAMETERS

Since not all of the parameters included in the mathematical model (13) can be easily isolated and measured, equation (13) was employed to identify the five unknown parameters c_0, c_1, $m\epsilon$, ω_c and η representing the frequency independent and the frequency dependent losses, the unbalance, the critical speed and the hysteretic damping coefficient.

The mass m was measured, while the polar inertia I_p was evaluated analytically starting from the geometrical dimensions and the material characteristics giving

$$m = 1{\cdot}36 \text{ kg}, \qquad I_p = 5{\cdot}1 \times 10^{-3} \text{ kg m}^2.$$

Experimental data obtained under different operating conditions of unbalance and cooling distance were analyzed using the identification procedure.

Experimental rundown data were obtained in a vacuum by accelerating the rotor up to a speed of about 5500 rpm. The rotor was then decoupled and the speed of the freely rotating disk was measured as a function of time.

Two different identification procedures were used: (i) *identification from the angular acceleration curves*—performed by minimizing the distance between the theoretical and experimental $(\omega, \dot{\omega})$ curves; (ii) *identification from the angular speed curves*—performed by minimizing the distance between the theoretical and experimental (t, ω) curves.

4.1. IDENTIFICATION FROM THE ANGULAR ACCELERATION CURVES

The angular acceleration was evaluated as the slope of a linear best fit to the $(t, \omega(t))$ curves obtained during rundown experiments. The computation was done within a "time window" of amplitude Δt sliding from the beginning to the end of the test record. The errors of this method are small if the angular acceleration is constant within the time window Δt. The linear data fitting with a constant value of Δt was then adopted only for rotor speeds far from the critical, so that the angular acceleration was low and slowly varying with time.

At speeds close to ω_c, the changes in the angular acceleration are faster. In this case, $\dot{\omega}$ was evaluated as the slope of a straight line connecting consecutive measurements at times t_k and t_{k+1}:

$$\dot{\omega}(t_k) = \frac{\omega(t_{k+1}) - \omega(t_k)}{t_{k+1} - t_k}. \tag{16}$$

This is equivalent to a reduction of Δt to its minimum value.

The frequency independent and the frequency dependent loss coefficients c_0 and c_1 were identified by a linear approximation of the $(\omega, \dot{\omega})$ curve at speeds much lower than the critical, where the rundown equation (13) reduces to equation (14).

Taking equation (13) into account, the maximum value of the contribution to the angular acceleration due to the unbalance is reached at a value ω_{pk}:

$$\omega_{pk} = \omega_c \sqrt{1 + \eta^2}, \tag{17}$$

such that

$$(I_p\dot{\omega} - c_0 - c_1\omega)_{pk} = -\frac{1}{m}\,\omega_{pk}^2 (m\epsilon)^2 \frac{1}{\eta}. \tag{18}$$

The left side of equation (18) can be determined from the experimental curves and from parameters c_0 and c_1, previously identified. The value of the damping parameter is then

$$\eta = -\frac{\omega_{pk}^2 (m\epsilon)^2}{m(I_p\dot{\omega} - c_0 - c_1\omega)_{pk}}. \tag{19}$$

Substituting equations (19) and (17) into equation (13), the unbalance can be obtained as a function of the rotational speed. The nearly constant value of the unbalance identified in the speed range 2000–5000 rpm was considered as a proof of the identification method.

In Table 1 are shown the parameters identified from experimental data obtained for different values of the unbalance and of the cooling distance. While the critical speed ω_c, $|c_0|$ and $|c_1|$ are found to decrease with increasing cooling distance, the hysteretic damping coefficient η was practically constant. As expected, all balanced configurations show an identified unbalance that is considerably lower than the unbalanced ones. The variation of the unbalance with the cooling distance can be due to slight changes in the location of the elastic axis of the bearing from experiment to experiment when the cooling distance was changed.

The continuous curves of Figure 3 show the experimental (t, ω) data obtained with a cooling distance of 4 mm, while the dashed ones were obtained by numerical integration of equation (13) using the estimated parameters of Table 1. The value of the rotating speed measured at the beginning of the test has been assumed as initial condition for the integration.

4.2. IDENTIFICATION FROM THE ANGULAR SPEED RUNDOWN CURVES

In the previous identification procedure, equation (13) is considered as an explicit link between angular acceleration and angular speed and is based on a data fitting procedure of $(\omega, \dot{\omega})$ curves derived directly from the experimental (t, ω) rundown curves. In the

TABLE 1

Parameters identified from the angular acceleration curves

Cooling distance (mm)	Balancing (y/n)	Pressure (10^{-4} torr)	c_0/I_p $\left(10^{-3}\,\frac{\text{rad}}{\text{s}^2}\right)$	c_1/I_p $\left(10^{-6}\,\frac{1}{\text{s}}\right)$	ω_c (rad/s)	$m\epsilon \pm \sigma_{m\epsilon}$ (g mm)	η
1·6	n	7	−19·0	−60·0	133·0	640·0 ± 9·0	0·16
4·0	n	5	−2·8	−44·0	85·0	650·0 ± 16·0	0·17
6·0	n	2	−2·2	−36·0	71·0	560·0 ± 36·0	0·12
1·6	y	9·0 ± 1·0	−29·0	−60·0	140·0	220·0 ± 5·0	0·08
4·0	y	7·0 ± 1·0	−4·9	−44·0	92·0	290·0 ± 4·0	0·11
6·0	y	4	−2·2	−36·0	71·0	313·0 ± 10·0	0·11

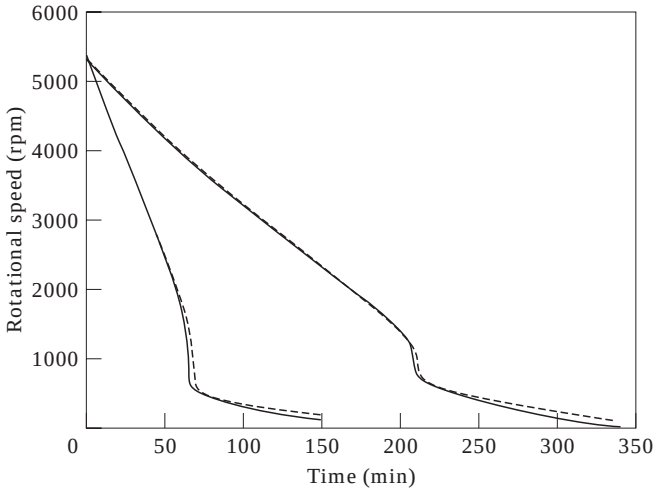

Figure 3. Experimental (continuous) versus simulated rundown curves (dashed), identified from the angular acceleration: 4 mm cooling distance. The upper curves are for the balanced rotor and the lower curves for the unbalanced rotor.

following, equation (13) is considered as a differential equation that is numerically integrated within the time interval t_0, t_{end} corresponding to the duration of the test.

The value of the maximum rotating speed ω_0 at the beginning of a test is assumed as initial condition at time t_0 for the numerical integration, performed using a standard second or third order Runge–Kutta routine. This leads to a theoretical rundown curve $\omega_{th}(t_i)$ evaluated at discrete time steps t_i. The theoretical rundown curve is considered as a function of the system parameters c_0, c_1, η, ω_c and $m\epsilon$.

The identified set of the system parameters is computed as that which minimizes the error function $E(c_0, c_1, \eta, \omega_c, m\epsilon)$, defined as the mean square of the relative error between the experimental (subscript *exp*) and the theoretical (subscript *th*) values of the rotating speed at times t_i:

$$E(c_0, c_1, \eta, \omega_c, m\epsilon) = \frac{1}{n}\sqrt{\sum_{i=1}^{n}\left(\frac{\omega_{th}(t_i) - \omega_{exp}(t_i)}{\omega_{exp}(t_i)}\right)^2}. \tag{20}$$

The identification routine is based on the following step-wise procedure. (1) For a given set of the system parameters, the theoretical rundown curve $\omega_{th}(t_i)$ is computed by numerical integration of equation (13) within the time interval t_0, t_{end}. (2) The error function $E(c_0, c_1, \eta, \omega_c, m\epsilon)$ is computed. (3) A new set of parameters $c_0, c_1, \eta, \omega_c, m\epsilon$ is determined to minimize the error E.

Points (1), (2) and (3) are iterated until the error function of equation 20 converges to a minimum value within a given tolerance. The minimum search routine exploits the functions implemented in the optimization toolbox of the Matlab software [18] and is based on a Levenberg–Marquardt method with a mixed quadratic and cubic search procedure.

The parameters of Table 1 have been adopted as starting guess for the minimization algorithm. This choice has shown to be the less prone to make the routine converge to physically meaningless parameter sets.

TABLE 2

Parameters identified from the angular speed curves

Cooling distance (mm)	Balancing (y/n)	Pressure (10^{-4} torr)	c_0/I_p $\left(10^{-3}\,\frac{\text{rad}}{\text{s}^2}\right)$	c_1/I_p $\left(10^{-6}\,\frac{1}{\text{s}}\right)$	ω_c (rad/s)	$m\epsilon$ (g mm)	η
1·6	n	7	−28·0	76·0	123·0	655·0	0·16
4·0	n	5	−6·7	−52·0	90·0	652·0	0·17
6·0	n	2	−5·4	52·0	74·0	761·0	0·13
1·6	y	9·0 ± 1·0	−33·0	−27·0	136·0	215·0	0·14
4·0	y	7·0 ± 1·0	−6·6	−33·0	88·0	239·0	0·14
6·0	y	4	−2·3	−35·0	65·0	307·0	0·14

The values obtained from the identification procedure are reported in Table 2 as a function of cooling distance and balancing conditions. Physically, both parameters c_0 and c_1 have to be positive as they represent the drag torques due to the frequency dependent and the frequency independent loss mechanisms. The positive signs of c_1/I_p for the unbalanced rotor and cooling distances of 1·6 and 6 mm are probably due to numerical inaccuracies in the identification procedure due to the small relevance of the aerodynamic, eddy current and magnetic friction losses compared to the losses from magnetic unbalance.

All of the curves of Figure 4 are relative to a cooling distance of 4 mm; the continuous curves show the experimental rundown data for the balanced and the unbalanced rotor. The dashed curves are obtained by numerical integration of equation (13) with the identified parameters listed in Table 2. The upper dashed curve is obtained from the theoretical model with the parameter values of the balanced configuration except for the unbalance which was reduced by 50% to 118 g mm.

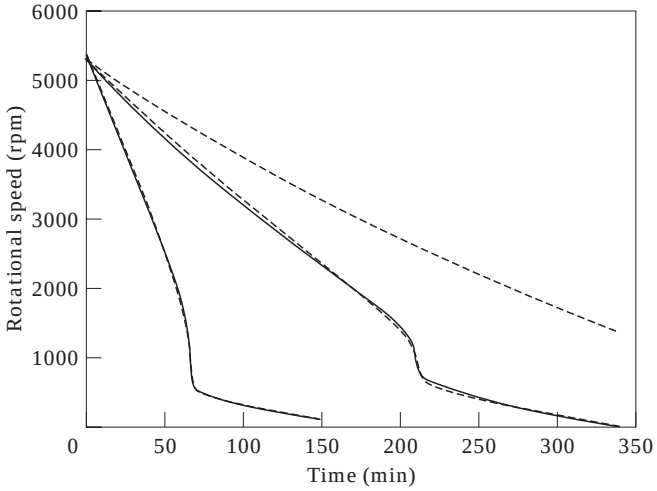

Figure 4. Experimental (continuous) versus identified rundown curves (dashed) identified by relative error minimization: 4 mm cooling distance. The upper curves are relative to the balanced rotor and the lower curves are for the unbalanced rotor. The upper dashed curve was calculated using the theoretical model with parameters of the balanced configuration and an unbalance reduced by 50%.

From the analysis of Figure 4, it is clear that in supercritical conditions the main source of energy dissipation is due to the combined effects of the flywheel unbalance and of the hysteretic characteristic of the superconducting bearing. This energy dissipation occurs not only in the vicinity of the critical speeds but also above it. Good balancing of the rotor–bearing system can therefore be very effective to reduce the long-term energy losses in the system.

5. CONCLUSIONS

We have investigated the loss mechanisms in a superconducting flywheel system due to the combined effects of magnetic unbalance and hysteretic damping. The analysis was performed under the assumption that the bearing characteristics can be modelled as a linear, elastic, isotropic spring with structural damping.

The parameters of the system were identified in two different ways: (1) by the analysis of the rotational speed–angular acceleration curves; and (2) by minimizing the mean square value of the relative error between theoretical model and the time–speed experimental data. The good approximation that can be obtained by the theoretical model, and the reasonable consistency of the parameters identified by two different methods, is considered as a validation of the modelling procedure.

In addition to magnetic friction and eddy current losses, the hysteretic nature of the superconducting bearing makes a significant contribution to the overall losses, as it dissipates energy whenever the rotor is subject to a whirling motion on a plane perpendicular to its axis. The amplitude of this whirling motion is a function of the unavoidable eccentricity between the flywheel centre of gravity and the elastic axis of the magnetic suspension. Due to the low stiffness values that are usually obtained for superconducting bearings and the need to operate at high speeds to optimize the kinetic energy stored in the flywheel, these systems are usually operated in supercritical conditions. In order to increase the efficiency of the system, it is of crucial importance to reduce the unbalance of the rotor supported by the bearings. This is achieved by minimizing the distance between centre of gravity and the elastic axis of the rotor.

REFERENCES

1. E. H. Brandt 1988 *Applied Physics Letters* **53**, 1554–1556. Friction in levitated superconductors.
2. J. R. Hull, T. M. Mulcahy, L. Lynds, B. R. Weinberger, F. C. Moon and P. Z. Chang 1990 *Proceedings of the* 25*th IECEC Conference*, 432–436. Phenomenology of forces acting between magnets and superconductors.
3. G. Genta 1995 *Vibration of Structures and Machines*. New York: Springer-Verlag: second edition.
4. C. Delprete, G. Genta, L. Mazzocchetti, E. Rava, A. Ricca and G. Ripamonti 1992 *Proceedings of the* 3*rd International Symposium on Magnetic Bearings*, 287–296. High speed asynchronous motor with high T_c superconducting bearings.
5. B. R. Weinberger, L. Lynds, J. R. Hull and U. Balachandran 1991 *Applied Physics Letters* **59**, 1132–1134. Low friction in high temperature superconductor bearings.
6. V. V. Nemoshkalenko, E. H. Brandt, A. A. Kordyuk and B. G. Nikitin 1990 *Physica C* **170**, 481–485. Dynamics of a permanent magnet levitating above a high-T_c superconductor.
7. P. Boegler, C. Urban, H. Rietschel and H. J. Bornemann 1994 *Applied Superconductivity* **2**, 315–325. Standardized measurements of interaction forces in autostable superconducting magnetic bearings.
8. H. J. Bornemann, P. Boegler, R. Zabka, H. Rietschel, P. de Rango, X. Chaud, P. Gautier-Picard and R. Tournier 1993 *Applied Superconductivity*. YBCO texturation and applications of superconducting magnetic bearings in flywheels for energy storage.

9. H. J. Bornemann, C. Urban, P. Boegler, T. Ritter, O. Zaitsev, K. Weber and H. Rietschel 1994 *Physica C* **235**, 3455–3456. High speed superconducting flywheel system for energy storage.
10. H. J. Bornemann, T. Ritter, C. Urban, O. Zaitsev, K. Weber and H. Rietschel 1994 *Applied Superconductivity* **2**, 439–447. Low friction in a flywheel system with passive superconducting magnetic bearings.
11. A. Chambers, A. D. Chew and A. P. Troup 1992 *Journal of Vacuum Science Technology A* **10**, 2655–2660. Rotating disc gauge for absolute total pressure measurement in high vacuum.
12. F. C. Moon 1990 *International Journal of Applied Electromagnetics in Materials* **1**, 29–35. Magnetic forces in high-T_c superconducting bearings.
13. H. J. Bornemann, C. Urban, P. Boegler, H. Kupfer and H. Rietschel 1993 in *Advances in Superconductivity IV* (T. Fujita and Y. Shiohara, editors) **2**, 1311–1316. Melt-textured Y–Ba–Cu–O and its applications to autostable superconducting bearings.
14. P. Z. Chang, F. C. Moon, J. R. Hull and T. M. Mulcahy 1990 *Journal of Applied Physics* **67**, 4358–4360. Levitation force and magnetic stiffness in bulk high-temperature superconductors.
15. F. C. Moon, K. C. Weng and P. Z. Chang 1989 *Journal of Applied Physics* **66**, 5643–5645. Dynamic magnetic forces in superconducting ceramics.
16. F. C. Moon, M. M. Yanoviak and R. Ware 1988 *Applied Physics Letters* **52**, 1534–1536. Hysteretic levitation forces in superconducting ceramics.
17. R. Albanese, C. Delprete, G. Genta, A. Tonoli, L. Mazzocchetti and E. Rava 1994 *Proceedings of the 4th International Symposium on Magnetic Bearings*, 417–422. Design, construction and testing of a kinetic energy storage device with high T_c superconductive suspension.
18. A. Grace 1992 *Matlab Optimization Toolbox User's Guide*. Natick, Massachusetts: The Mathworks, Inc.

APPENDIX: NOMENCLATURE

c_0	coefficient of the frequency independent losses
c_1	coefficient of the frequency dependent losses
n	number of samples during the rundown tests
m	flywheel mass
t	time
x, y	displacements of the elastic axis of the flywheel
z	complex co-ordinate
B	magnetic flux density
B_z	gradient of B in circumferential direction
C	bearing elastic axis
E	mean square of the error between experimental and theoretical rundown curves
F	bearing force
HTS	high T_c superconductor
K	bearing stiffness
I_p	flywheel polar inertia moment about its axis
LN_2	liquid nitrogen
P	dissipated power
Q_ϑ	Lagrangian component of the forces about the axis of the flywheel
W	dissipated power
T	kinetic energy
T_c	critical temperature
Z_0	whirling amplitude
ϵ	flywheel eccentricity
φ	whirling phase angle
ρ	electric resistivity
ϑ	rotation angle about the flywheel axis
ω	flywheel rotating speed
ω_c	flywheel critical speed
Γ	drag torque

Subscripts

brg	bearing
ec	eddy current
diss	dissipated
k	*k*th time step
pk	peak
th	theoretical
α	circumferential direction
exp	experimental